IEEE Access
Multidisciplinary | Rapid Review | Open Access Journal

Received 27 June 2024, accepted 22 July 2024, date of publication 25 July 2024, date of current version 5 August 2024.

Digital Object Identifier 10.1109/ACCESS.2024.3433528

RESEARCH ARTICLE

A Wideband Single-Feed Circularly Polarized Stacked Patch Antenna

GIACOMO MUNTONI[1], (Member, IEEE), GIOVANNI ANDREA CASULA[1], (Senior Member, IEEE), MANUELA TRAVERSARI[2], AND GIORGIO MONTISCI[1], (Senior Member, IEEE)

[1]Dipartimento di Ingegneria Elettrica ed Elettronica, Università degli Studi di Cagliari, 09123 Cagliari, Italy
[2]Settimo San Pietro, 09060 Cagliari, Italy

Corresponding author: Giorgio Montisci (giorgio.montisci@unica.it)

ABSTRACT We present a circularly polarized single-feed stacked patch antenna with wide axial ratio bandwidth, suitable for both coaxial probe feeding and coplanar microstrip feeding. The antenna is composed of two patches with truncated corners connected together using four pins. The circularly polarized antenna has been designed using CST Studio Suite in the upper part of the UHF frequency band. A prototype has been fabricated using low-cost 3D-printing manufacturing technology. In this regard, both the dielectric substrate and the support for the stacked patches have been realized with a 3D-printed Polylactic Acid. Measured results provide a 34% −10 dB reflection coefficient bandwidth (between 2.14 and 3.03 GHz) and a 3 dB axial ratio bandwidth of 25% (between 2.31 and 2.97 GHz), with a flat gain in the overlapped (axial ratio-reflection coefficient) bandwidth that coincides with the axial ratio bandwidth and a peak gain of 8.5 dBic.

INDEX TERMS Circular polarization, microstrip antennas, patch antennas, wide bandwidth.

I. INTRODUCTION

Circularly polarized (CP) microstrip patch antennas are very popular thanks to their low profile, low-cost, light weight, and ease of fabrication. On the other hand, the main limitation associated with CP patch antennas is the narrow axial ratio (AR) bandwidth [1].

The bandwidth of CP patch antennas can be improved by employing dual-feed or multi-feed excitations, wherein additional feeding networks are required [2], [3]. Single-feed patch antennas based on defected ground plane configurations [4], [5], [6] can also be employed, ensuring an AR bandwidth up to 60% at the expense of a high back-radiation and low gain, making these antennas not suitable for the realization of directive patch arrays. Therefore, in this paper we will focus on conventional (i.e., with a solid ground plane) single-feed microstrip patch antennas. Several solutions have been proposed in the literature to improve their AR bandwidth.

The E-shaped configurations presented in [7] and [8] provide an AR bandwidth close to 10% using patches suspended on thick air substrates and sustained by the feeding coaxial probe. Stacked ring patches [9] or stacked patches with other shapes [10] have also been proposed, with an AR bandwidth still less than 10%.

A further enhancement of the AR bandwidth can be obtained using a meandering strip probe to feed the patch, as made in [11] and [12]. Specifically, in [11] a 22% AR bandwidth is achieved, but the antenna performance is very sensitive to the meandering strip feed deployed in air. In [12], the meandering strip feed is made of printed strips and via holes on a multilayer substrate, ensuring a stable and robust solution. This antenna reaches an AR bandwidth of 16.8%, though the implementation could be cumbersome due to both the necessity of a multilayer substrate and the presence of via holes. Moreover, the antenna multilayer substrate is quite thick and could increase the dielectric losses.

In [13], a truncated corners patch with parasitic elements printed on a 1mm-thick PTFE substrate, suspended on a thick air substrate, is proposed, reaching an AR bandwidth of 23.9%.

In [14], the characteristic mode analysis is used to design an E-shaped patch with an AR bandwidth up to 25%. However, this antenna is printed on a thick dielectric substrate, which could increase the dielectric losses and the effect of the surface wave. In [15], a U-shaped stacked patch

The associate editor coordinating the review of this manuscript and approving it for publication was Ali Karami Horestani.

TABLE 1. Comparison between circularly polarized patch antennas with single-feed configuration (λ_0 is the free-space wavelength at the design center frequency).

Ref.	AR bandwidth (overlapped with S_{11}) (%) Simulated/Measured	Gain (max-min) (measured) (dBic)	Substrate thickness (patch region)	Substrate thickness (region surrounding the patch)	Feeding	Antenna configuration
[7]	8.1/9.3	7-8.3	0.09 λ_0	NA (suspended patch)	Coaxial	E-shaped patch
[8]	8/7	8-8.7	0.09 λ_0	NA (suspended patch)	Coaxial	E-shaped patch
[9]	8/7.7	6.6-7.3	0.1 λ_0	0.01λ_0	Coaxial	Stacked rings
[10]	13/10	5.6-6.3	0.2 λ_0	0.1 λ_0	Coaxial	Stacked patches
[11]	21.5/22.4	7.3-8.2	0.135 λ_0	0.017 λ_0	Coaxial	Meandering probe feed deployed in air
[12]	16.8/16.8	6.2-6.7	0.114 λ_0	0.114 λ_0	Coaxial	Meandering printed probe feeding
[13]	20.9/23.9	7.8-8.6	0.13 λ_0	NA (suspended patch)	Coaxial	Parasitic elements
[14]	19.5/25	5.0-7.3	0.114 λ_0	0.114 λ_0	Coaxial	E-shaped
[15]	52.7/52.7	5.2-8.3	0.226 λ_0	NA (suspended patch)	Coaxial	Stacked patches
[16]	27.6/27.6	2.5-5.3	0.045 λ_0	NA	Coaxial	Stacked patches and P.I.N. diodes
This work	25.2/25	7.8-8.5	0.135 λ_0	0.017 λ_0	Coaxial or coplanar microstrip	Stacked patches

antenna is presented by the same authors of [14]. A bandwidth of more than 50% is achieved. This is not surprising since the element stacking is obtained using foam and air with a thick substrate (0.226 λ_0) and the low-profile feature is definitely lost with this configuration.

In [16], a stacked configuration with multiple resonators is proposed, achieving an AR bandwidth of 27.6%. Both LHCP and RHCP have been obtained, but using lumped components (MACOM MA4GP907 P.I.N. diodes) and vias. As a consequence, a quite complicate realization is proposed, mainly due to the use of the P.I.N. diodes that need DC bias lines to set their on/off state. This could make the realization of planar arrays using such antennas very cumbersome, since the bias lines on the front side would degrade the array radiation pattern (see Fig. 10b of [15]). Moreover, a poor realized gain, ranging from 2.5 dBic to 5.3 dBic in the operating bandwidth, is observed in comparison with both our antenna and the other configurations analyzed here (see Table 1).

Based on the above considerations, the antennas proposed in [11], [12], [13], and [14] are the most promising single-feed CP antennas employing a conventional microstrip layout. However, the sensitivity of the antenna performance to the meandering strip fed deployed in air reduces the effectiveness of the configuration in [11] at higher frequencies. On the other hand, an improved solution with a similar configuration has been proposed in [12], using the same feeding strategy.

The antennas in [12], [13], and [14] provide a relatively simple and low-profile configuration, an AR bandwidth larger than 16% and a peak gain between 6.2 and 8.6 dBic.

Unfortunately, as apparent in the comparison reported in Table 1, most of the single-feed wideband CP antennas available in the literature are intended to coaxial feeding, whereas coplanar microstrip feeding is rarely used.

However, the most common and performing solution for the realization of beam forming networks of linear and planar arrays of patch antennas relies on coplanar microstrip feeding. In this regard, the antenna in [12] could be redesigned for coplanar microstrip feeding, likely maintaining the same performance, though it may require a separate microstrip network in the underneath [17] that could increase the back-radiation. On the other hand, the printed patch suspended on a thick air substrate of [13], the E-shaped patch printed on a thick dielectric substrate of [14], the suspended stacked patch of [15], and the stacked configuration of [16] allow only the coaxial probe feeding.

In this paper, we present a CP single-feed stacked patch antenna on a conventional microstrip substrate (see Fig. 1). It is composed of a first patch with truncated corners [18] with a stacked patch above, having truncated corners as well, connected to the lower patch by four pins. The main advantage of the proposed configuration is the position of the feeding point that is close to the edge of the lower patch, external to it and in a short stretch of a microstrip line, thus allowing to feed the antenna either with a coaxial probe (Fig. 1a) or with a coplanar microstrip line (Fig. 1c). The same electromagnetic performance is achieved independently of the selected feeding without any necessity of redesign, but using the same geometry fed either with a coaxial cable or with a coplanar microstrip line.

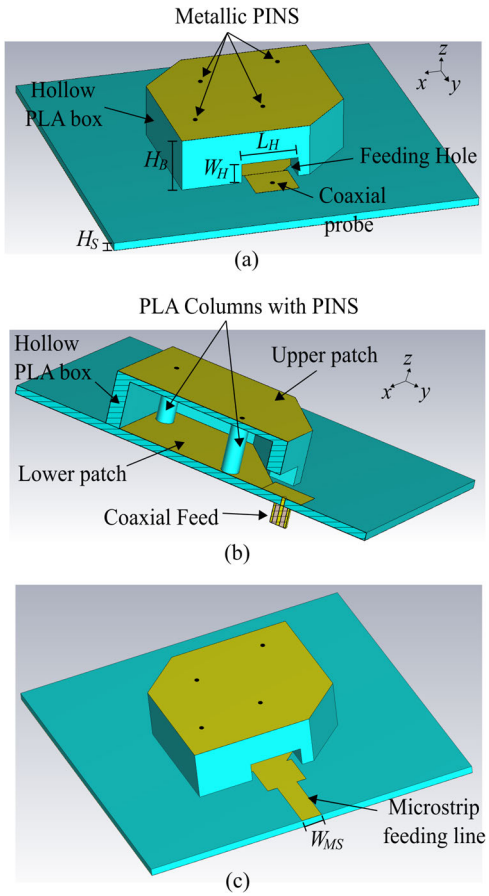

FIGURE 1. Layout of the proposed CP antenna: (a) 3D view with coaxial feeding; (b) 3D sectional view; (c) 3D view with coplanar microstrip feeding line.

In Table 1, we summarize the comparison between the configuration proposed in this work and the conventional single-feed CP microstrip antennas with wide AR bandwidth discussed above.

The losses in the substrate of our antenna are not critical since the stacking is limited to the region of the patches (see Fig. 1), whereas the thickness of the surrounding substrate can be selected as thin as necessary, depending on the operating frequency, dielectric permittivity, and dielectric loss tangent. In this regard, in Table 1, the thickness of the antenna substrate is explicitly reported for the analyzed configurations, both in the patch region and in the region surrounding it, to highlight the importance of this parameter when the CP antenna must be used in an array. In fact, a thick dielectric substrate could be acceptable in the region of the patch but should be avoided in the region surrounding the patch since this would increase the dielectric losses, hindering the use of a coplanar microstrip feeding network.

The above features of the proposed CP antenna add to its excellent electromagnetic performance, with a measured AR bandwidth of 25% a high gain stability in the operating band, and a peak gain of 8.45 dBic. The AR bandwidth is better or comparable with that of the antennas reported in Table 1, except for the antenna in [15] that reaches 52.7% AR

TABLE 2. Main features of CP patch antennas with single-feed.

	Realization complexity	Low profile	Realization of planar arrays with coplanar microstrip feeding
[11]	Moderate	Acceptable (0.13 λ_0)	Possible (to be redesigned - difficult at higher frequency)
[12]	Moderate	Acceptable (0.11 λ_0)	Possible (to be redesigned - increase back radiation)
[13]	Low	Acceptable (0.13 λ_0)	Not suitable
[14]	Low	Acceptable (0.11 λ_0)	Not suitable
[15]	Low	Poor (0.23 λ_0)	Not suitable
[16]	High	Good (0.045 λ_0)	Not suitable
Our work	Low	Acceptable (0.13 λ_0)	Yes

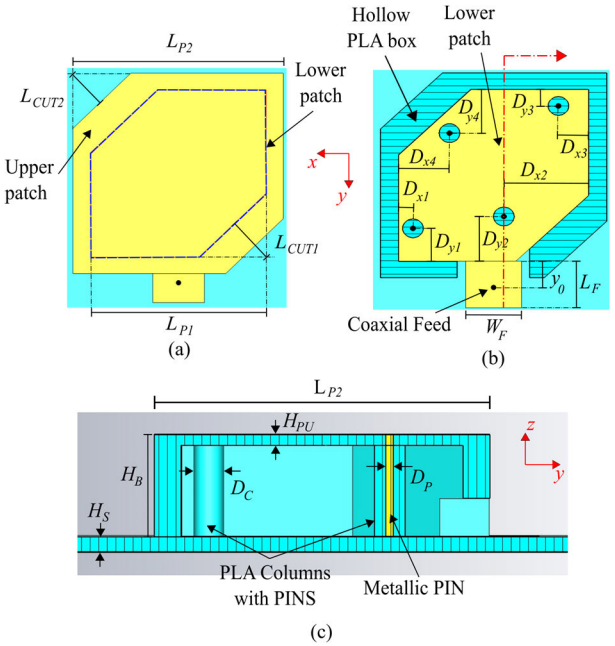

FIGURE 2. Geometry of the proposed antenna: (a) top view; (b) section view (xy plane); (c) section view (yz plane).

bandwidth, but at the expense of a very thick substrate. This makes our antenna a valuable alternative to the configurations available in the literature as a stand alone antenna, and a more convenient solution over [11], [12], [13], [14], [15], [16] as the element of planar arrays, thanks to both the thin substrate surrounding the patch and the coplanar microstrip feeding (see Fig. 1c).

To further highlight the advantages of our single-feed CP antenna, in Table 2 the main features of the configurations available in the literature are summarized.

Design and simulations of the proposed configuration have been performed using the commercial software CST Studio Suite and a prototype have been manufactured using 3D-printing additive manufacturing. Excellent agreement is observed between simulated and measured results.

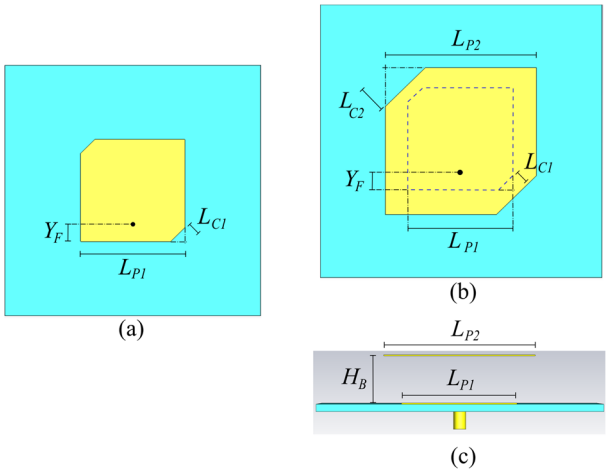

FIGURE 3. Single patch with truncated corners (a); configuration with stacked patches (top view) (b); configuration with stacked patches (side view) (c).

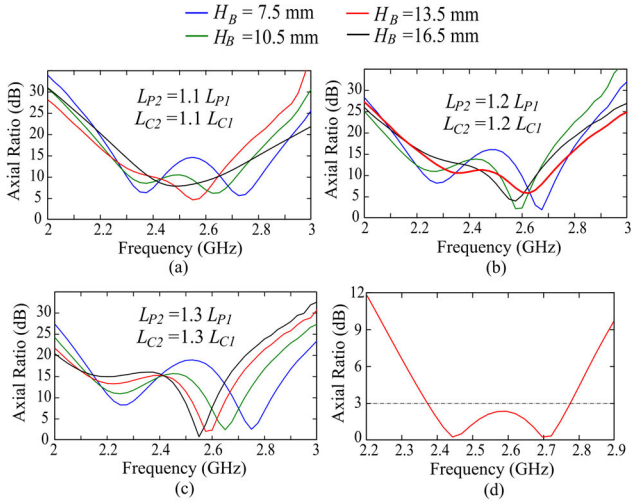

FIGURE 4. Parametric curves for the AR of the stacked configuration in Fig. 3 (a), (b), and (c); AR of the optimized stacked configuration in Fig. 3 (d).

II. ANTENNA DESIGN AND SIMULATIONS

The geometry of the proposed CP patch antenna is depicted in Figs. 1 and 2. In its basic configuration, it is composed of a first patch with truncated corners fed by a coaxial probe, and a stacked patch with truncated corners as well, sustained by a 3D-printed Polylactic Acid (PLA) support, and connected to the lower patch by four metallic pins housed into PLA columns.

The antenna design has been performed using the commercial software CST Studio Suite. The dielectric substrate (90 mm × 90 mm) and the support for the stacked patch are made of PLA with a dielectric permittivity of 2.55 and a loss tangent equal to 0.008 at 2.5 GHz. The thickness of the dielectric substrate H_S is set to 2 mm. The diameter of the metallic pins D_P is set to 1 mm, the diameter of the PLA columns D_C (surrounding and supporting the pins) is set to 4 mm, and the upper wall of the PLA box H_{PU} is 1.5 mm (see Fig. 2c).

In this section, we will describe the design procedure that leads to the proposed configuration, aiming to achieve the widest operating frequency bandwidth (within the pre-established range 2 GHz - 3 GHz) for both the AR and the reflection coefficient. The design steps are listed in the following.

A. DESIGN STEP 1

First, to obtain circular polarization, we design a standard square patch with truncated corners (see section 14.7 of [18]) fed by a coaxial probe, close to the patch edge [18], on a PLA substrate of thickness H_S (Fig. 3a). The patch length is half a guided wavelength at the center frequency (selected here equal to 2.5 GHz), and the truncated corners depth is optimized to achieve circular polarization. The outcome is a patch with the following geometry (see Fig. 3a): $L_{P1} = 36.7$ mm, $L_{C1} = 2.5$ mm, $Y_0 = 8.38$ mm. The AR bandwidth exhibits the narrowband typical value of 1.25%, with a −10 dB reflection coefficient bandwidth of 4%.

B. DESIGN STEP 2

A stacked patch with side L_{P2} and truncated corners L_{C2}, centered with respect to the first patch, is added at a distance H_B from the first patch (see Figs. 3b and 3c). This second patch acts as a parasitic element, thus the AR bandwidth enhancement is achieved by properly overlapping the AR frequency bands of the two patches. At this design step, the available design parameters are L_{P1}, L_{C1}, L_{P2}, L_{C2}, H_B, and Y_F. To simplify the design, the side of the first patch L_{P1} is set to the initial value of 36.7 mm and maintains this value throughout the rest of the design procedure.

In Fig. 4 the AR of the structure shown in Figs. 3b and 3c is reported for three different values of the resonant length of the second patch L_{P2}. Namely, L_{P2} is set respectively 10%, 20% and 30% longer than L_{P1}, varying the distance between the patches H_B from 7.5 mm to 16.5 mm. Initially, the truncated corner depth L_{C2} is scaled as L_{P2}, i.e., 10%, 20% and 30% larger than L_{C1}.

From Fig. 4, it can be seen that the two patches introduce two minima of the AR, whose spacing can be tuned by modifying the vertical distance H_B between the patches. The values of the AR between the two minima are high for all the reported curves, but they can be lowered below 3 dB by adequately tuning the truncated corner depths, L_{C1} and L_{C2}, as we will show later in this section.

At this stage, we select the values of L_{P2}, L_{C2}, and H_B, aiming to obtain a reasonable distance between the minima of the AR, with a value as low as possible for both the two minima and the peak between the minima. Based on this criterion, the best curves are the green curve of the Fig. 4a and the red curve of the Fig. 4b. We have selected the red curve in Fig. 4b, since it exhibits a slightly larger spacing between the minima. This choice corresponds to $L_{P2} = 44$ mm, $L_{C2} = 3.25$ mm, and $H_B = 13.5$ mm. H_B and L_{P2} are fixed here

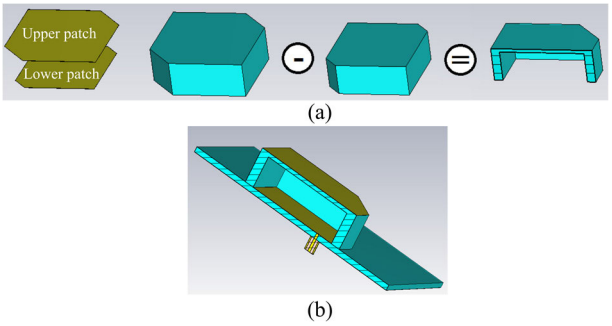

FIGURE 5. Construction of the hollow box supporting the upper patch (a); Stacked patch configuration with 3D printed hollow PLA box (b).

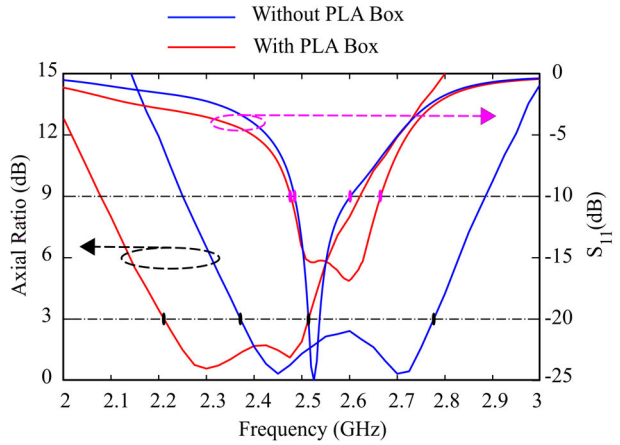

FIGURE 6. Axial Ratio and reflection coefficient of the stacked patch configuration, with and without the PLA box.

and maintain their value throughout the rest of the design procedure.

C. DESIGN STEP 3

We optimize the truncated corner depths L_{C1} and L_{C2} to achieve a 3 dB AR bandwidth as large as possible. This leads to $L_{C1} = 5$ mm and $L_{C2} = 4$ mm. Using these values, we obtain the AR shown in Fig. 4d, with an operating frequency band of 400 MHz (16%) that confirms the effectiveness of the proposed design strategy.

D. DESIGN STEP 4

The stacked patch must be sustained by an appropriate structure. To this purpose, a 3D printed hollow PLA box has been employed to support the suspended patch. This is an easy, cheap and robust solution to implement the antenna design (see Figs. 1 and 2). The internal contour of the hollow PLA box matches the lower patch, while supporting the stacked patch, which lies on the upper side of the box. Then, the PLA box is constructed by subtracting from the parallelepiped of height H_B, having the upper patch as base, a parallelepiped of height H_B-H_{PU}, having the lower patch as base (see Fig. 5a). The upper wall of the box H_{PU} is set to 1.5 mm.

The AR of the proposed antenna after the insertion of the PLA box is obviously degraded. Specifically, the dielectric

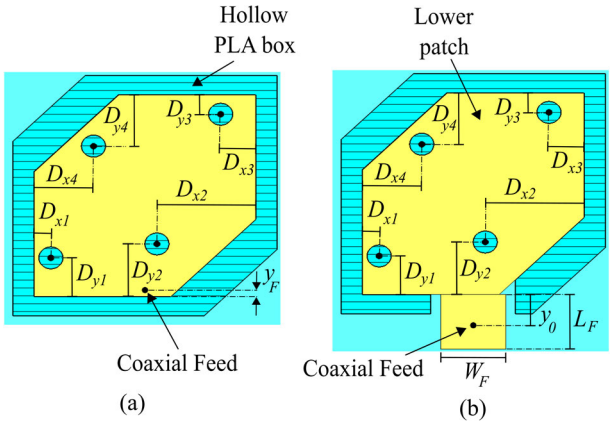

FIGURE 7. Section view (xy plane) of the antenna after insertion of the pins: (a) coaxial feeding of the lower patch without short matching line; (b) coaxial feeding of the lower patch with short matching line.

box has the effect of reducing the AR bandwidth and shifting the response to lower frequencies. The comparison between the ARs with and without the PLA box is shown in Fig. 6. Despite the presence of the hollow PLA box (and the consequent frequency shift), an AR bandwidth of 300 MHz (13%) is still achieved. On the other hand, the input matching cannot be obtained in the whole AR frequency band, but only in a little portion of it. The best result, obtained by moving the coaxial feed a bit closer to the antenna border ($Y_F = 6.35$ *mm*) (see Fig. 6), exhibits a -10 dB S_{11} frequency band of only 180 MHz (from 2.48 GHz to 2.66 GHz, equal to 7%).

E. DESIGN STEP 5

To further improve the AR bandwidth and ease the impedance matching, the two patches have been connected together using four metallic pins (see Figs. 1, 2, and 7). Each pin (of diameter $D_P = 1$ mm) is surrounded by a hollow PLA cylinder (of diameter $D_C = 4$ mm) with the main purpose of providing a straight path for it and giving mechanical robustness to the structure. A few iterations are required to obtain the optimal position of the pins (see Fig. 7a). The starting point of this optimization procedure is $D_{xi} = 9$ mm, $D_{yi} = 9$ mm, $i = 1,\ldots,4$. Since the pins modify the surface current distribution on the patches, at each iteration the truncated corner depths L_{C1} and L_{C2} should be tuned, too.

The values of the geometrical parameters optimized at this final design step are: $L_{C1} = 10.8$ mm, $L_{C2} = 8.2$ mm, $D_{x1} = 2.8$ mm, $D_{y1} = 7$ mm, $D_{x2} = 16.4$ mm, $D_{y2} = 9.5$ mm, $D_{x3} = 5.8$ mm, $D_{y3} = 3.5$ mm, $D_{x4} = 9.8$ mm, $D_{y4} = 9.3$ mm, with $Y_F = 1$ mm. The corresponding AR and the reflection coefficient are reported in Fig. 8 (red curves).

Regarding the input matching, we have found that moving the coaxial feeding point very close to the edge of the patch, up to the limit of $Y_F = 1$ mm (Fig. 7a), the reflection coefficient exhibits a flat behaviour in the AR bandwidth, thought its value does not lower below -5 dB (see the red curve in Fig. 8a). This impedance mismatch is

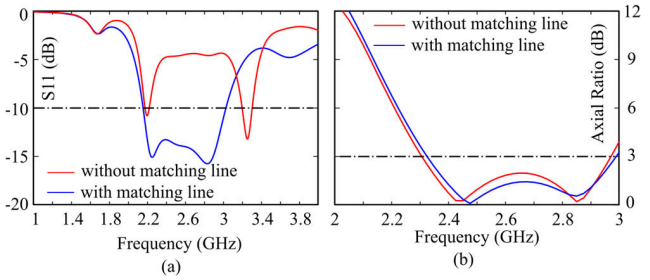

FIGURE 8. Reflection coefficient (a) and Axial Ratio (b) of the designed antenna with (Fig. 7b) and without (Fig. 7a) the short matching line.

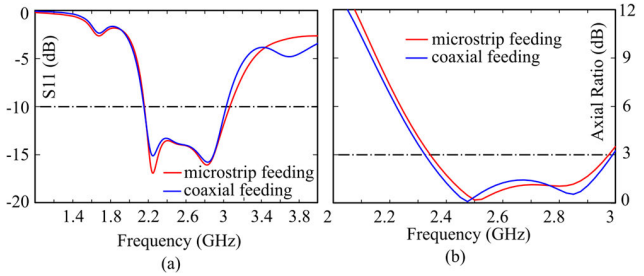

FIGURE 9. Reflection coefficient (a) and Axial Ratio (b) of the designed antenna with coaxial feeding (Fig. 1a) and with a 50 Ω coplanar microstrip feeding line (Fig. 1c).

mainly due to an inductive input impedance of the antenna. Therefore, we compensate this effect with a capacitive matching provided by a short and wide microstrip line [19] (of length L_F and width W_F, see Fig. 7b).

The final results with L_F=10 mm, $W_F = 10.8$ mm, and $Y_0 = 6$ mm are reported in Fig. 8 (blue curves). A hole of size $L_H = 14$ mm $\times$ $W_H = 5$ mm (see Fig. 1a) is made in the hollow PLA box in correspondence to the matching line to ease the soldering of the coaxial cable. It can be noticed that the insertion of the capacitive matching does not modify the AR and provides a wideband behaviour for the reflection coefficient, which covers the AR bandwidth. In fact, the simulated -10 dB bandwidth of the reflection coefficient is about 34% (from 2.15 to 3.03 GHz), the simulated 3 dB AR bandwidth is 25.2% (from 2.32 to 2.99 GHz), and the overlapped bandwidth is 25.2%.

The proposed antenna can be fed also using a coplanar microstrip configuration as shown in Fig. 1c. This is achieved by simple accessing the 50 Ω feeding point with a coplanar microstrip line instead of a coaxial probe. Therefore, a 50 Ω feeding line of width 5.5 mm is used in place of the coaxial feed, leaving the geometry unmodified. As reported in Fig. 9, the antenna performance is virtually the same.

Finally, the simulated realized gain is stable within the axial ratio bandwidth, with a peak value of 8.5 dBic (see Fig. 14), and the simulated radiation efficiency is also stable at around 95% (see Fig. 10).

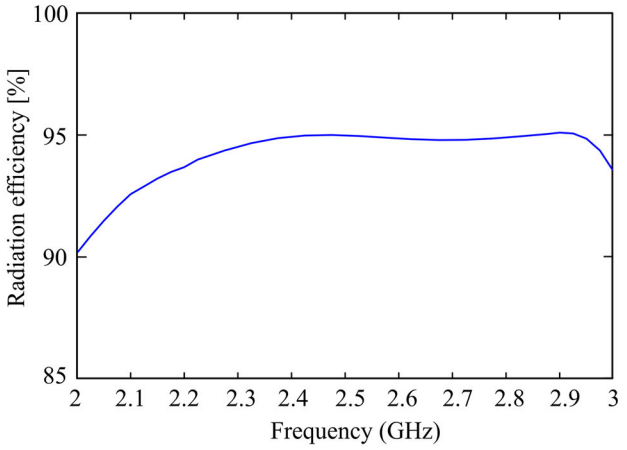

FIGURE 10. Simulated radiation efficiency of the proposed antenna with coaxial feeding.

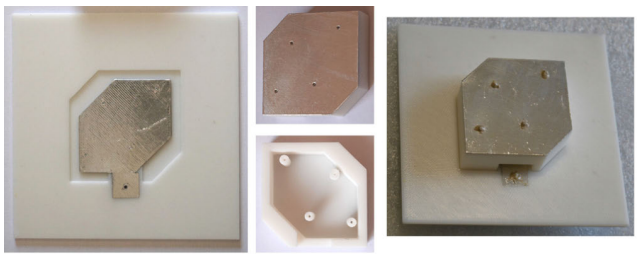

FIGURE 11. 3D-printed parts of the designed antenna (a); prototype of the designed antenna (b).

III. ANTENNA FABRICATION AND EXPERIMENTAL VERIFICATION

An antenna prototype has been fabricated using the commercial 3D-printer PRUSA MK3S+ and a PLA thermoplastic filament. The metallization of the ground plane and patches has been realized using 50 μm-thick adhesive aluminum tape, cut with the cutting machine Cricut maker®. The coaxial connector has been glued to the aluminum tape by using a silver-loaded conductive epoxy adhesive.

In Fig. 11a the (metalized) 3D-printed parts of the antenna are shown, whereas in Fig. 11b the assembled prototype is depicted.

The electromagnetic performance of the manufactured prototype has been measured in an anechoic environment (Fig. 12) by using the Anritsu MS46322B two-port vector network analyzer. The AR and the broadside realized gain of the antenna under test (AUT) have been measured using a known-gain horn antenna (range antenna) according to the definitions reported in Secs. 8 and 9 of [20].

In Fig. 13 the reflection coefficient is reported, showing a good agreement between simulation and measurement with a measured bandwidth between 2.14 GHz and 3 GHz. In Fig. 14 the broadside realized gain and the AR are shown. The agreement between simulation and measurement is still very good. The measured 3 dB AR bandwidth ranges from 2.31 GHz to 2.97 GHz with a 25% fractional bandwidth. The measured antenna gain is stable in the 3 dB AR bandwidth, ranging from 7.8 dBic to 8.45 dBic.

Finally, in Fig. 15 the CST simulated far-field pattern at 2.40 GHz, 2.65 GHz, and 2.90 GHz is depicted. The

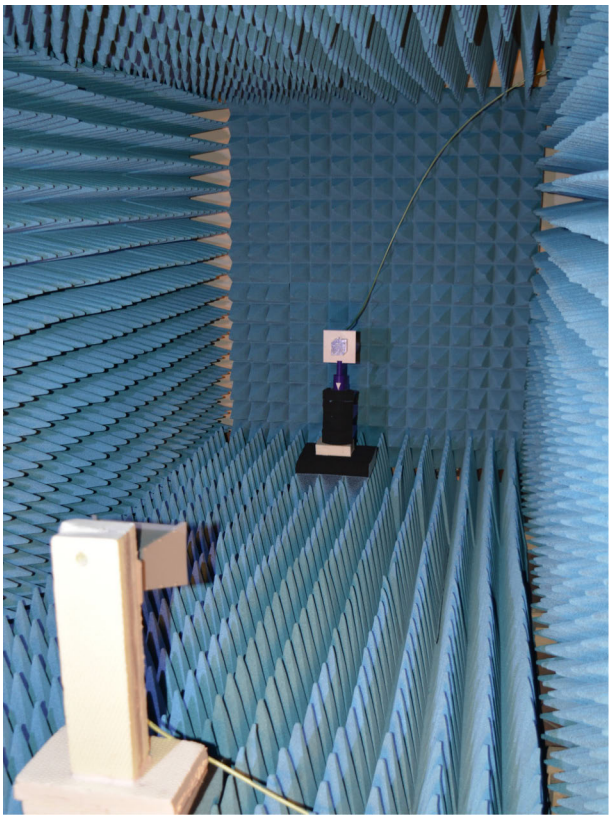

FIGURE 12. Experimental setup for the measurement of the realized gain and axial ratio.

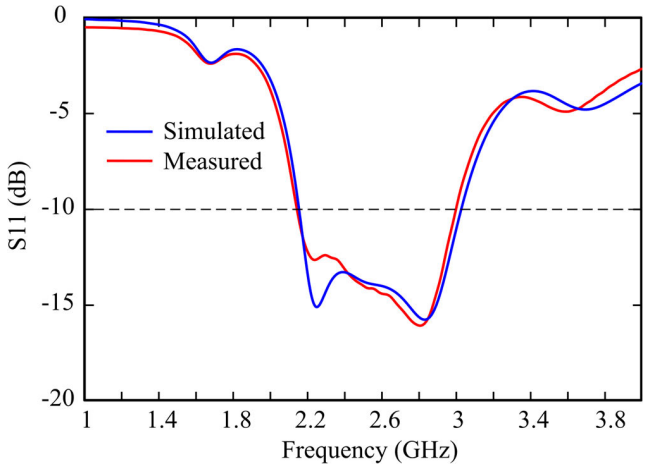

FIGURE 13. Comparison between simulated and measured reflection coefficient of the manufactured prototype.

simulated half-power beamwidths (HPBWs) for the left hand circular polarization (LHCP) in the xz- and yz- planes are, respectively, 67.8° and 68° at 2.40 GHz, 64° and 63.4° at 2.65 GHz, 57.7° and 61° at 2.90 GHz. The simulated front-to-back ratio for the LHCP is 28 dB at 2.40 GHz, 26 dB at 2.65 GHz, and 28 dB at 2.90 GHz.

In Fig. 15, the measured LHCP and RHCP components are reported only in the broadside direction according to the experimental setup in Fig. 12, which does not allow an accurate measurement of the far-field pattern at scanning angles.

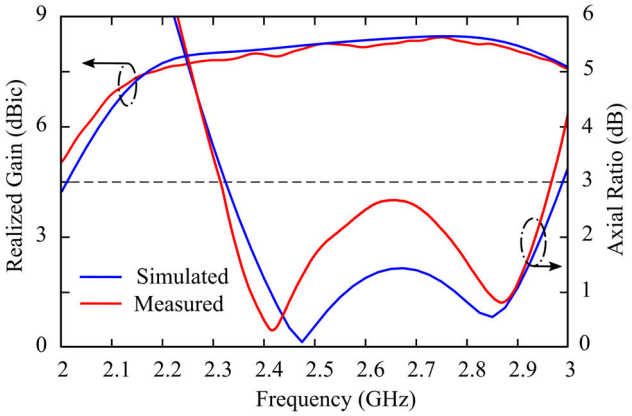

FIGURE 14. Comparison between simulated and measured realized gain and axial ratio of the manufactured prototype.

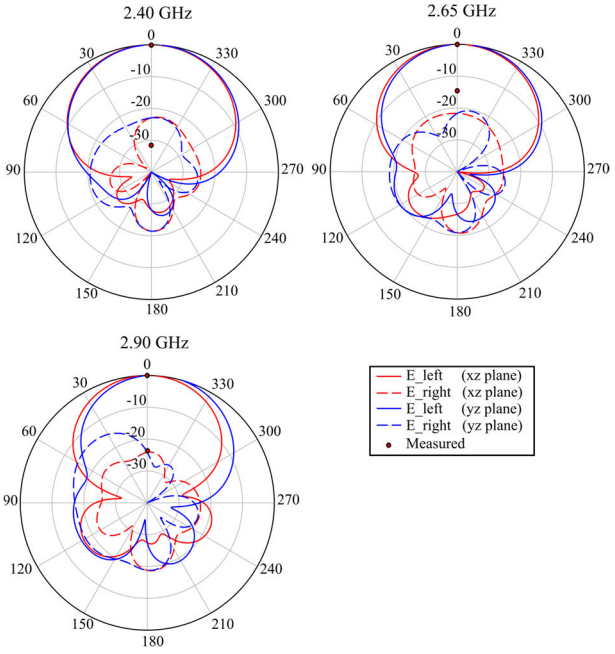

FIGURE 15. Simulated far-field pattern at 2.4 GHz, 2.65 GHz, and 2.90 GHz.

IV. CONCLUSION

A novel CP stacked patch antenna with single-feed and wide AR bandwidth is proposed in this work. The main distinctive feature of the presented configuration consists of providing a wide AR bandwidth (greater than or comparable to similar configurations available in the literature), while allowing feeding flexibility (coaxial probe or coplanar microstrip feeding). Specifically, the same electromagnetic performance is achieved regardless of the selected feeding method without the necessity of redesign, using the same geometry fed either with a coaxial cable or a coplanar microstrip line.

Easy and economic fabrication is achieved thanks to the use of 3D-printing technology. A measured 3 dB AR bandwidth of 25% is achieved with a peak gain of 8.5 dBic. This is an excellent performance for a single-feed CP antenna realized on a conventional microstrip substrate, i.e., with a solid ground plane.

Moreover, the stacking is limited to the region of the patches, whereas the thickness of the surrounding substrate could be selected as thin as necessary, depending on the operating frequency, dielectric permittivity, and dielectric loss tangent. This allows to reduce both the losses in the substrate and the effect of the surface wave.

Thanks to the wide CP bandwidth, the high gain and efficiency, and the feeding flexibility, the proposed antenna is a good candidate for the realization of planar arrays for broadband CP applications.

REFERENCES

[1] S. Gao, Q. Luo, and F. Zhu, *Circularly Polarized Antennas*. Hoboken, NJ, USA: Wiley, 2014.

[2] R. Caso, A. Buffi, M. R. Pino, P. Nepa, and G. Manara, "A novel dual-feed slot-coupling feeding technique for circularly polarized patch arrays," *IEEE Antennas Wireless Propag. Lett.*, vol. 9, pp. 183–186, 2010.

[3] C.-F. Liang, Y.-P. Lyu, D. Chen, and C.-H. Cheng, "Wideband circularly polarized stacked patch antenna based on TM11 and TM10," *IEEE Trans. Antennas Propag.*, vol. 70, no. 4, pp. 2459–2467, Apr. 2022.

[4] H. Bagheroghli, "A novel circularly polarized microstrip antenna with two connected quasi monopoles for wideband applications," *IEEE Antennas Wireless Propag. Lett.*, vol. 12, pp. 1343–1346, 2013.

[5] T. Fujimoto and K. Jono, "Wideband rectangular printed monopole antenna for circular polarisation," *IET Microw., Antennas Propag.*, vol. 8, no. 9, pp. 649–656, Jun. 2014.

[6] M. Nosrati and N. Tavassolian, "Miniaturized circularly polarized square slot antenna with enhanced axial-ratio bandwidth using an antipodal Y-strip," *IEEE Antennas Wireless Propag. Lett.*, vol. 16, pp. 817–820, 2017.

[7] A. Khidre, K. Fang Lee, F. Yang, and A. Elsherbeni, "Wideband circularly polarized E-shaped patch antenna for wireless applications," *IEEE Antennas Propag. Mag.*, vol. 52, no. 5, pp. 219–229, Oct. 2010.

[8] A. Khidre, K.-F. Lee, F. Yang, and A. Z. Elsherbeni, "Circular polarization reconfigurable wideband E-shaped patch antenna for wireless applications," *IEEE Trans. Antennas Propag.*, vol. 61, no. 2, pp. 960–964, Feb. 2013.

[9] T.-N. Chang and J.-M. Lin, "Circularly polarized ring-patch antenna," *IEEE Antennas Wireless Propag. Lett.*, vol. 11, pp. 26–29, 2012.

[10] Y.-X. Guo and D. C. H. Tan, "Wideband single-feed circularly polarized patch antenna with conical radiation pattern," *IEEE Antennas Wireless Propag. Lett.*, vol. 8, pp. 924–926, 2009.

[11] X. H. Tang, Y. L. Long, H. Wong, and K. L. Lau, "Broadband circularly polarized patch antenna with 3D meandering strip feed," *Electron. Lett.*, vol. 47, no. 19, pp. 1060–1062, Sep. 2011.

[12] Q. W. Lin, H. Wong, X. Y. Zhang, and H. W. Lai, "Printed meandering probe-fed circularly polarized patch antenna with wide bandwidth," *IEEE Antennas Wireless Propag. Lett.*, vol. 13, pp. 654–657, 2014.

[13] J. Wu, Y. Yin, Z. Wang, and R. Lian, "Broadband circularly polarized patch antenna with parasitic strips," *IEEE Antennas Wireless Propag. Lett.*, vol. 14, pp. 559–562, 2015.

[14] J. Zeng, X. Liang, L. He, F. Guan, F. H. Lin, and J. Zi, "Single-fed triple-mode wideband circularly polarized microstrip antennas using characteristic mode analysis," *IEEE Trans. Antennas Propag.*, vol. 70, no. 2, pp. 846–855, Feb. 2022.

[15] J. Zeng, Z. Zhang, F. H. Lin, and F. Guan, "Penta-mode ultrawideband circularly polarized stacked patch antennas using characteristic mode analysis," *IEEE Trans. Antennas Propag.*, vol. 70, no. 10, pp. 9051–9060, Oct. 2022.

[16] M. Li, Z. Zhang, M.-C. Tang, L. Zhu, and N.-W. Liu, "Bandwidth enhancement and size reduction of a low-profile polarization-reconfigurable antenna by utilizing multiple resonances," *IEEE Trans. Antennas Propag.*, vol. 70, no. 2, pp. 1517–1522, Feb. 2022.

[17] H. W. Lai, D. Xue, H. Wong, K. K. So, and X. Y. Zhang, "Broadband circularly polarized patch antenna arrays with multiple-layers structure," *IEEE Antennas Wireless Propag. Lett.*, vol. 16, pp. 525–528, 2017.

[18] C. A. Balanis, *Antenna Theory Analysis and Design*, 3rd ed., Hoboken, NJ, USA: Wiley, 2006.

[19] D. M. Pozar, *Microwave Engineering*. Hoboken, NJ, USA: Wiley, 2011.

[20] *IEEE Recommended Practice for Antenna Measurements*, IEEE Standard 149, 2021.

GIACOMO MUNTONI (Member, IEEE) received the bachelor's degree in electronic engineering, the master's degree in telecommunication engineering, and the Ph.D. degree in electronic engineering and computer science from the University of Cagliari, in 2010, 2015, and 2019, respectively.

He is currently a Technologist with the Applied Electromagnetics Group, University of Cagliari. His research interests include the design and characterization of antennas for biomedical and aerospace applications, microwave-based dielectric characterization of materials, 3D printing of RF components, and monitoring of the space debris environment in low Earth orbit with the Sardinia Radio Telescope, in collaboration with Cagliari Astronomical Observatory.

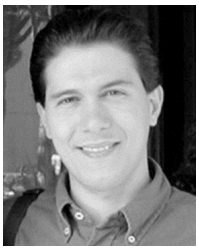

GIOVANNI ANDREA CASULA (Senior Member, IEEE) received the M.S. degree in electronic engineering and the Ph.D. degree in electronic engineering and computer science from the University of Cagliari, Cagliari, Italy, in 2000 and 2004, respectively.

Since December 2017, he has been an Associate Professor of electromagnetic fields with the University of Cagliari, teaching courses in electromagnetics and antenna engineering. He has authored or co-authored about 50 articles in international journals. His current research interests include the analysis and design of waveguide slot arrays, RFID antennas, wearable antennas, and numerical methods in electromagnetics. He is an Associate Editor of IEEE TRANSACTIONS ON ANTENNAS AND PROPAGATION, *IET Microwaves, Antennas and Propagation*, *Electronics* (MDPI), and *Sensors* (MDPI); and an Academic Editor of *International Journal of Antennas and Propagation*.

MANUELA TRAVERSARI received the degree in electronic engineering from the University of Cagliari, in 2005. She is currently a High School Teacher of information technology.

GIORGIO MONTISCI (Senior Member, IEEE) received the M.S. degree in electronic engineering and the Ph.D. degree in electronic engineering and computer science from the University of Cagliari, Cagliari, Italy, in 1997 and 2000, respectively. Since February 2022, he has been a Full Professor of electromagnetic fields with the University of Cagliari, teaching courses in electromagnetics and microwave engineering. He has authored or co-authored 86 articles in international journals. His current research interests include the analysis and design of waveguide slot arrays, RFID antennas, wearable antennas, numerical methods in electromagnetics, and microwave circuits and systems. He received IEEE Access Outstanding Associate Editor, in 2020, 2021, and 2023. He is an Associate Editor of IEEE ACCESS and *IET Electronics Letters* and an Academic Editor of *International Journal of Antennas and Propagation*.

Open Access funding provided by 'Università degli Studi di Cagliari' within the CRUI CARE Agreement